Viscous effects on flows through pressure-swirl atomizers

E. Wimmer, G. Brenn*
Institute of Fluid Mechanics and Heat Transfer, Graz University of Technology, Austria
wimmer@fluidmech.tu-graz.ac.at and brenn@fluidmech.tu-graz.ac.at

Abstract

We analyse theoretically the flow through the swirl chamber of a pressure-swirl atomizer with the aim to explain the counter-intuitive phenomenon that, for a given driving pressure difference across a given atomizer, a liquid with a higher viscosity is put through at a higher flow rate than a less viscous liquid. We decompose the flow field into three zones and model the pressure losses across the two outer zones empirically. For the inner zone, we solve the transport equations for mass and momentum under appropriate simplifications and obtain a theoretical description of the flow field in this zone adjacent to the air core. A formulation of the mass flow rate as a function of the driving pressure difference defines the discharge coefficient as a function of the atomizer geometry and the relevant liquid properties. For comparison with the computational results, experiments on the discharge behaviour of pressure-swirl atomizers were carried out. Results from the calculations reproduce the experimentally observed liquid flow rates well. Data from other authors also fit well. The theoretical description of the flow field in the swirl chamber allows the discharge behaviour to be related to the air-core diameter.

Introduction

Pressure-swirl atomizers are widely used in various industrial applications for their reliability in operation, and for the high liquid throughput paired with fine drop size of the sprays. Pressure-swirl atomizers are the standard atomizers in many spray-drying processes of, e.g., the chemical and food industries. An essential part of this kind of atomizers is a swirl generator which forces the process liquid into a rotating motion. The swirl may be imposed by an insert in the axial feed line inside the atomizer, or by tangential feed of the liquid into a swirl chamber. In both cases the liquid leaves the atomizer through a fine orifice in the form of an annular liquid sheet, which diverges in flow direction, assuming a conical shape with decreasing thickness as the distance from the orifice increases.

The liquid flow rate through the atomizer depends, of course, on the driving pressure difference across the atomizer, the relevant properties of the atomizer geometry, and the liquid properties density and dynamic viscosity. One marked property of the flow through pressure-swirl atomizers, which is yet unexplained, is the fact that, for a given atomizer geometry and at a given driving pressure difference, the throughput of a liquid with a higher liquid viscosity is higher than for a less viscous liquid. This behaviour of viscous liquid flows through swirl chambers, which is counter-intuitive at the first glance, is the subject of the present investigation.

The flow field in swirl chambers of various kinds of apparatus, such as gas centrifuges and atomizers, has been the subject of research and development since many decades. Taylor investigated the evolution of the boundary layer in a pressure-swirl atomizer [1]. Neglecting the axial velocity component against the dominant swirling component, he found that, starting from the entry into the swirl chamber, the boundary layer grows to a maximum thickness and, towards the orifice, it thins again, so that for a fluid with the viscosity of water, forced through an orifice of 2mm by a driving pressure of 10 bar, the boundary layer extends inwards to a distance of 11 % of the radius of the orifice.

Chinn discussed in detail the inviscid flow through swirl nozzles, applying the principle of maximum flow to find the dimensions of the wall bounded film and various other properties of the flow through the atomizer for a given liquid throughput [2,3]. The author shows that, in some cases of geometries and liquids, the inviscid theoretical description of the flow field may quite closely describe the real flows found in experiments.

Quite some work on the flow problem at hand was carried out in the former Soviet Union. Goldshtik described the swirling gas flow in a swirl chamber, decomposing the flow field into two zones and, for calculating the flow fields in the various zones, simplifying the velocity fields and the underlying momentum equations [4]. Khavkin followed the same lines, but applied the method of Goldshtik to a liquid flow field with a free surface at an air core around the symmetry axis of the swirl chamber [5]. The most important result of his work is the description of the discharge coefficient of the flow through the swirl chamber as a function of the geometry and relevant physical data of the liquid. In their derivation, Khavkin et al. applied a coupling condition for zone boundaries taken from Goldshtik's work for a single-phase flow field to the free surface of the liquid in contact with the air core, which must be considered with care [6].

In our present contribution we describe theoretically the flow through the swirl chamber of a pressure-swirl atomizer, modelling a part of the pressure losses empirically and solving the transport equations for mass and momentum under simplifications appropriate for the inner zone of the flow field. The simplifications may be introduced due to the

* Corresponding author: brenn@fluidmech.tu-graz.ac.at

negligibility of one velocity component. Having arrived at a description of the discharge behaviour of the atomizer, we study the dependency of the results on various parameters. We then compare the computational results to data from a series of experiments. We aim to explain the phenomenon that, at a given driving pressure difference, a liquid with a higher viscosity results in a higher throughput through the atomizer than a less viscous liquid. The paper ends with the conclusions from our work.

Theoretical investigation of the flow field in the swirl chamber

We describe theoretically the flow through the swirl chamber of a pressure-swirl atomizer, decomposing the flow field into three zones: (1) one radial outer zone at large distances from the axis of symmetry of the flow field, close to the swirl chamber wall, (2) one zone next to the first zone, covering the entrance port of the swirl chamber, and (3) one zone bounded downstream by the air core of the flow field [6]. We model empirically the pressure losses in zones (1) and (2) and solve the transport equations for mass and momentum under simplifications appropriate for zone (3). The simplifications are needed since the flow field is in general three-dimensional and very complicated. We arrive at a theoretical description of the flow field in the third zone, which allows us to relate the flow rate to the driving pressure difference for varying liquid properties and atomizer geometry.

The structure of the swirl chamber and the various zones of the flow field are shown in Fig. 1. It is seen that the swirl chamber exhibits cylindrical symmetry and has one inlet port with the width d_{in}. The diameter of the chamber is $2R_0$, the height is L. We present the analysis of the flow fields in the three zones, following the lines of Khavkin et al. [6].

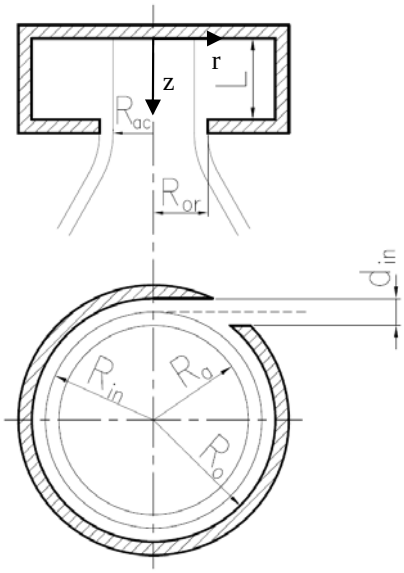

Figure 1. Structure of the swirl chamber and the three zones of the flow field; coordinate system.

Zone 1: $R_0 \geq r \geq R_{in}$

The entrance of the flow, from the tangential port into the swirl chamber is hydrodynamically complex. Novikov suggests to restrict the description of this zone of the flow field to quantifying the pressure losses at the inlet port as per [7]

$$\Delta p_1 = p_0 - p_{in} = \zeta_1 \frac{\rho u_{in}^2}{2} \tag{1}$$

where p_0 is the liquid pressure upstream from the inlet of the atomizer, where the velocity is small, and p_{in} is the liquid pressure at the radial position $r = R_{in}$. The coefficient ζ_1 represents the hydrodynamic losses in the flow through the inlet port.

Zone 2: $R_{in} \geq r \geq R_a (= R_{in} - d_{in}/2)$

Since the flow in this zone is very complicated, the relation between the liquid velocity at the inlet port and the tangential velocity u_a at the boundary $r = R_a$ of the zone is quantified by the hydraulic coefficient

$$\Psi = \frac{u_a R_a}{u_{in} R_{in}} \tag{2}$$

which is the ratio of angular momentum in the two states and is later determined empirically. The pressure at the position $r = R_a$ is calculated by the extended Bernoulli equation

$$p_{in} + \rho \frac{u_{in}^2}{2} = p_a + \rho \frac{u_a^2}{2}\left(1 + \zeta_2\right) \tag{3}$$

Combining equations (2) and (3) allows for the elimination of the velocity u_a, so that we obtain

$$\Delta p_2 = p_{in} - p_a = \left(\Psi^2 \frac{R_{in}^{\ 2}}{R_a^{\ 2}}\left(1 + \zeta_2\right) - 1 \right) \rho \frac{u_{in}^2}{2} \tag{4}$$

for the pressure loss across zone 2. The loss coefficient ζ_2 remains to be determined.

Zone 3: $R_a \geq r \geq R_{ac}$

In zone 3, which extends from $r = R_a$ to the radius R_{ac} of the air core, we analyse the velocity field accounting for the influence of the viscous interaction of the flow with the swirl chamber walls by a modelling approach. For this purpose, Khavkin et al. [6] use the equation of Blasius for turbulent flow in a smooth-walled straight pipe. Khavkins et al.'s theory predicts the mass flow rate quite well, but by making the following adjustments we were able to enhance the accuracy. In our variant of Khavkin et al.'s model, the viscous stress at the top and bottom swirl chamber walls is modelled by the Blasius flat-plate boundary layer theory, which leads to the equation

$$\tau_0 = 0.664\,\mathrm{Re}^{-1/2}\,\frac{\rho u^2}{2} \tag{5}$$

for the local wall shear stress with

$u = \sqrt{u_\Theta^2 + u_r^2}$, and $\mathrm{Re} = \frac{uL}{\nu} = \frac{u_{in}L}{\nu}\Psi\frac{R_{in}u}{R_a u_a} = \mathrm{Re}_{in}\,\Psi\frac{R_{in}u}{R_a u_a}$

For the radial and angular components of the wall shear stress in a cylindrical coordinate system, Khavkin et al. set the following expressions [6]:

$$\tau_r = \tau_0\frac{u_r}{u}\ ; \qquad \tau_\Theta = \tau_0\frac{u_\Theta}{u} \tag{6}$$

In zone 3, $|u_\Theta| >> |u_r|$. Therefore the velocity may be approximated as $u = u_\Theta$. Equation (6) then becomes

$$\tau_r = \frac{0.664}{\mathrm{Re}_{in}^{1/2}}\frac{\rho}{2}\left(\frac{1}{\Psi}\frac{R_a}{R_{in}}\right)^{1/2}\frac{u_\Theta u_r}{(u_\Theta/u_a)^{1/2}}; \qquad \tau_\Theta = \frac{0.664}{\mathrm{Re}_{in}^{1/2}}\frac{\rho}{2}\left(\frac{1}{\Psi}\frac{R_a}{R_{in}}\right)^{1/2}\frac{u_\Theta^2}{(u_\Theta/u_a)^{1/2}} \tag{7}$$

Zone 3 exhibits a 2-D rotating flow field with $u_r = f_r(r)$, $u_\Theta = f_\Theta(r)$, $u_z = 0$. With account for the viscous interaction of the fluid with the swirl chamber walls, the equations of motion read

continuity
$$\frac{1}{r}\frac{d(r\,u_r)}{dr} = 0 \tag{8}$$

θ momentum
$$u_r\frac{d(ru_\Theta)}{dr} = -\frac{2\tau_\Theta r}{\rho L} \tag{9}$$

r momentum
$$u_r\frac{du_r}{dr} - \frac{u_\Theta^2}{r} = -\frac{1}{\rho}\frac{dp}{dr} - \frac{2\tau_r}{\rho L} \tag{10}$$

From the continuity equation we obtain immediately the radial velocity component u_r as

$$u_r = -\frac{\dot{m}}{2\pi r L\rho} = -u_{in}\frac{A_{in}}{2\pi r L} \tag{11}$$

where $\dot{m}$ is the liquid mass flow rate through the atomizer. Substituting equation (7) into equations (9) and (10) yields the balance equations for the radial and angular velocity components

$$u_r\frac{d(ru_\Theta)}{dr} = -\frac{r}{L}\frac{0.664}{\mathrm{Re}_{in}^{1/2}}\frac{1}{\Psi^{1/2}}\left(\frac{R_a}{R_{in}}\right)^{1/2}\frac{u_\Theta^2}{(u_\Theta/u_a)^{1/2}} \tag{12}$$

$$u_r\frac{du_r}{dr} - \frac{u_\Theta^2}{r} = -\frac{1}{\rho}\frac{dp}{dr} - \frac{1}{L}\frac{0.664}{\mathrm{Re}_{in}^{1/2}}\frac{1}{\Psi^{1/2}}\left(\frac{R_a}{R_{in}}\right)^{1/2}\frac{u_\Theta u_r}{(u_\Theta/u_a)^{1/2}} \tag{13}$$

For solving these equations in non-dimensional form, we introduce the definitions

$$\bar{u}_r = \frac{u_r}{u_a}; \qquad \bar{u}_\Theta = \frac{u_\Theta}{u_a}; \qquad \bar{p} = \frac{p}{\rho u_a^2}; \qquad x = \frac{r}{R_a}; \qquad \alpha = \frac{A_{in}}{2\pi R_{in} L}; \tag{14}$$

The non-dimensional form $\bar{u}_r$ of the solution (11) of equation (8) then reads

$$\bar{u}_r = -\frac{\alpha}{\Psi}\frac{1}{x} \tag{15}$$

Equation (12) becomes

$$\frac{d(x\bar{u}_\Theta)}{dx} = \beta\frac{\Psi^{1/2}}{\mathrm{Re}_{in}^{1/2}}x^2\,\bar{u}_\Theta^{3/2} \tag{16}$$

with $\beta = \dfrac{0.664\,R_a}{\alpha L}\left(\dfrac{R_a}{R_{in}}\right)^{1/2}$.

Equation (16) is a first-order nonlinear Bernoulli-type ordinary differential equation. With the boundary condition $\bar{u}_\Theta = 1$ at $x = 1$, the solution of (16) reads

$$\bar{u}_\Theta = \left[\left(-1-\frac{\beta}{3}\left(\frac{\Psi}{\mathrm{Re}_{in}}\right)^{1/2}\right)x^{1/2} + \frac{\beta}{3}\left(\frac{\Psi}{\mathrm{Re}_{in}}\right)^{1/2}x^2\right]^{-2} \tag{17}$$

With the two velocity components u_r and u_Θ known, we obtain from equation (13) the non-dimensional radial pressure gradient

$$\frac{d\,\bar{p}}{d\,x} = \frac{\alpha^2\beta}{\Psi^{3/2}\,\mathrm{Re}_{in}^{1/2}}\frac{\bar{u}_\Theta^{1/2}}{x} + \frac{\bar{u}_\Theta^{2}}{x} - \bar{u}_r\frac{d\,\bar{u}_r}{d\,x} \tag{18}$$

For determining the pressure p_a at the boundary between zones 2 and 3, equation (18) has to be integrated from $x=1$ to the position of the air core $x_{ac} = R_{ac}/R_a$. With the boundary condition $\bar{p} = \bar{p}_{amb}$ at $x = x_{ac}$, the pressure difference $p_a - p_{amb}$ becomes

$$p_a - p_{amb} = \rho\frac{u_{in}^2}{2}2\Psi^2\frac{R_{in}^2}{R_a^2}\left(\frac{\alpha^2\beta}{\Psi^{3/2}\,\mathrm{Re}_{in}^{1/2}}\int_{x_{ac}}^{1}\frac{\bar{u}_\Theta^{1/2}}{x}dx + \int_{x_{ac}}^{1}\frac{\bar{u}_\Theta^{2}}{x}dx - \frac{\alpha^2}{2\Psi^2}\left(1-\frac{1}{x_{ac}^2}\right)\right) \tag{19}$$

The radius of the air core is calculated by Khavkin [8] using an empirical correlation obtained from experiments with different atomizers, but always with water as the test liquid. In our approach the radius of the air core is calculated using the Bernoulli equation formulated for a streamline with negligible z velocity component between the state "a" and the surface of the air core. The velocities and pressures result from the above viscous calculations. With the velocity u_{ac} at the position $r = r_{ac}$ the equation reads

$$p_a + \frac{u_a^2}{2}\rho = p_{amb} + \frac{u_{ac}^2}{2}\rho \tag{20}$$

Assuming that the angular velocity component u_Θ at the air core is much larger than u_r, the pressure difference $p_a - p_{amb}$ becomes

$$\Delta p_3 = p_a - p_{amb} = \frac{\rho}{2}\left(u_\Theta^2 - u_a^2\right) \tag{21}$$

Rearranging equation (21) and using equation (17) leads to the requirement that

$$81R_a^2\,\mathrm{Re}_{in}^2\,u_a^2R_{ac}^{-2}\left(-3\sqrt{\mathrm{Re}_{in}} - \beta\sqrt{\Psi} + \left(\frac{R_{ac}}{R_a}\right)^{3/2}\beta\sqrt{\Psi}\right)^{-4} = \frac{2\Delta p_3}{\rho} + u_a^2 \tag{22}$$

The pressure difference Δp_3 across zone 3 is known as $\Delta p_3 = \Delta p - \Delta p_1 - \Delta p_2$, where $\Delta p = p_0 - p_{amb}$ is the total pressure difference across the atomizer. The radius of the air core R_{ac} is calculated as a solution of equation (22). We assume that the air core has the shape of a cylinder, so that its radius is constant over the height of swirl chamber. Accord-

ing to Orzechowski [9], at the final outlet from the atomizer the pressure across the emerging liquid film should be the ambient pressure p_{amb}. Here the centrifugal pressure is transformed into dynamic pressure, which leads to the formation of an axial velocity component u_z at the final outlet. The component u_z at the final outlet can be calculated as

$$u_z = \sqrt{u_{in}^2 2\Psi^2 \frac{R_{in}^2}{R_a^2}\left(\frac{\alpha^2\beta}{\Psi^{3/2}\,\mathrm{Re}_{in}^{1/2}}\int_{x_{ac}}^{1}\frac{\bar{u}_\Theta^{1/2}}{x}dx+\int_{x_{ac}}^{1}\frac{\bar{u}_\Theta^{2}}{x}dx-\frac{\alpha^2}{2\Psi^2}\left(1-\frac{1}{x_{ac}^2}\right)\right)-u_\Theta^2+u_a^2} \tag{23}$$

The mass flow rate through the orifice can then be formulated as

$$\dot{m} = 2\pi\rho\int_{r=R_{ac}}^{R_{or}} u_z\, r\, dr \tag{24}$$

With the calculated radius of the air core, and combining equations (23) and (24), the flow rate through the atomizer is

$$\dot{m} = 2\pi\rho R_a^2\int_{x=x_{ac}}^{x_{or}}\sqrt{u_{in}^2 2\Psi^2 \frac{R_{in}^2}{R_a^2}\left(\frac{\alpha^2\beta}{\Psi^{3/2}\,\mathrm{Re}_{in}^{1/2}}\int_{x_{ac}}^{1}\frac{\bar{u}_\Theta^{1/2}}{x}dx+\int_{x_{ac}}^{1}\frac{\bar{u}_\Theta^{2}}{x}dx-\frac{\alpha^2}{2\Psi^2}\left(1-\frac{1}{x_{ac}^2}\right)\right)-u_\Theta^2+u_a^2}\;\; x\,dx \tag{25}$$

For this calculation, the values of ζ_1, ζ_2 and Ψ must be known. According to the investigations of Khavkin [5], the flow through the tangential inlet port of the swirl atomizer may be approximated as a separated flow at the entrance into a duct. For this flow situation the value $\zeta_1 = 0.49$ may be used [7]. The values for Ψ and ζ_2 found by Khavkin et al. experimentally are determined by the relations [6]

$$\Psi = 1+(c_1\chi^2-1)e^{-c_2\chi} \tag{26}$$

$$\zeta_2 = c_3/\chi \tag{27}$$

where $\chi = \alpha\dfrac{R_a}{R_{in}}$

For the constants c_1, c_2 and c_3 Khavkin found experimentally the values c_1 = 30.6, c_2 = 50.4, c_3 = 0.061. We use these empirical data for our present study, since our atomizers are geometrically very similar to the ones used by Khavkin et al. [6].

Discharge Experiments with Pressure-Swirl Atomizers

In order to quantify the discharge behaviour of various pressure-swirl atomizers with varying liquids, we carried out a series of measurements. The atomizers were type Delavan SDX and Schlick 432 nozzles, which are widely in use, e.g., for spray drying applications. The geometries of the atomizers are shown in Figs. 2 and 3.

Figure 2. Geometry of the Delavan SDX atomizers (©Delavan Spray Technologies)

Figure 3. Geometry of the atomizer Schlick 432 (©Düsen-Schlick GmbH)

The relevant data of the swirl chambers used in the experiments are listed in Tables 1 and 2. The swirl chambers of the Delavan atomizers have one rectangular inlet into the swirl chamber, while the Schlick atomizer has two circular inlets. The atomizers were mounted on the spray test rig of the institute, which is used for characterising spray flows by

optical measuring techniques. For the purpose of the present measurements the test rig was just used for running the atomizers with the test liquids. For the liquid supply, a feeding pump, followed by a two-head piston pump, were used. In the low-pressure line, a flow rate meter (Endress + Hauser Promass 83; accuracy ±0.1 % of the measured value) working on the Coriolis principle was located for measuring the liquid throughput. The static pressure difference against atmosphere just upstream from the entrance into the atomizer was measured with a piezoelectric sensor (WIKA 5-11; 0-400 bar, accuracy 0.5% of span), so that the liquid throughput can be represented as a function of the driving pressure difference against the ambient air.

Table 1 Geometrical data of the Delavan and Schlick swirl chambers

Swirl chamber type	R_{in} [mm]	Swirl chamber height L [mm]	Swirl chamber inlet width d_{in} [mm]	Swirl chamber inlet area A_{in} [mm²]
Delavan – SB	6.33	1.23	1.61	1.98
Delavan – SC	5.60	1.36	2.45	3.33
Delavan – SD	5.60	1.88	2.45	4.61
Delavan – SE	5.60	2.67	2.45	6.54
Delavan – SF	4.92	3.77	3.2	12.06
Schlick 432 – 40	3.4	8.1	4	25.1

Table 2 Orifice diameters of the Delavan and Schlick atomizers

Orifice type	Orifice diameter D_{or} [mm]
Delavan - 30	0.762
Delavan - 40	1.016
Delavan - 50	1.27
Delavan - 60	1.524
Delavan - 70	1.778
Delavan - 90	2.286
Schlick 432 -1,5	1.5

A dimensional analysis yields the following parameters as relevant for the problem of liquid flow through the atomizer: mass flow rate $\dot{m}$, driving pressure difference Δp, liquid dynamic viscosity and density, μ_l and ρ, and the relevant geometrical parameters of the atomizer R_{in}, A_{in}, D_{or}. The analysis yields the non-dimensional representation of the liquid flow rate through the atomizers in the form [10]

$$\frac{\dot{m}}{\mu_l R_{in}} = 1.18 \left(\frac{D_{or}}{R_{in}} \right)^{1.34} \left(\frac{A_{in}}{R_{in}^{\ 2}} \right)^{0.35} \left(\frac{\sqrt{\Delta p \rho} R_{in}}{\mu_l} \right)^{0.885} \tag{28}$$

The throughput data for various liquids and atomizer geometries are shown in non-dimensional form in Fig. 3 as a comparison of measured data with results from eq. (28). The ranges of experimental data are listed in Table 3.

Results from Computation and Experiment

The discharge behaviour of the Delavan SDX atomizer SB-30 as a function of the liquid dynamic viscosity with the pressure difference as a parameter is shown in Fig. 4 in dimensional form. Here we see that, for the given atomizer, the throughput of a liquid with higher dynamic viscosity is significantly higher than with lower viscosity. This is the phenomenon we seek to represent by the present theory.

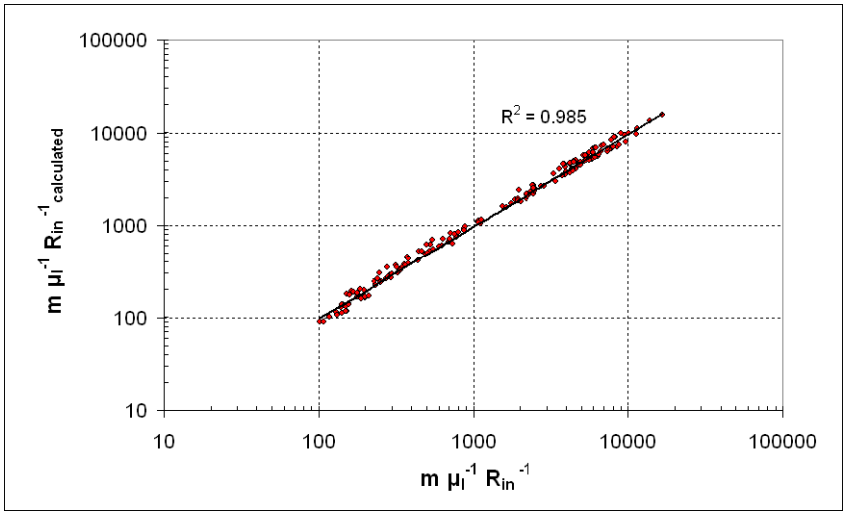

Figure 3. Comparison of measured liquid flow rates with results from eq. (28) for various combinations of swirl chambers and orifices (Tables 1 and 2) and the operation conditions in Table 4

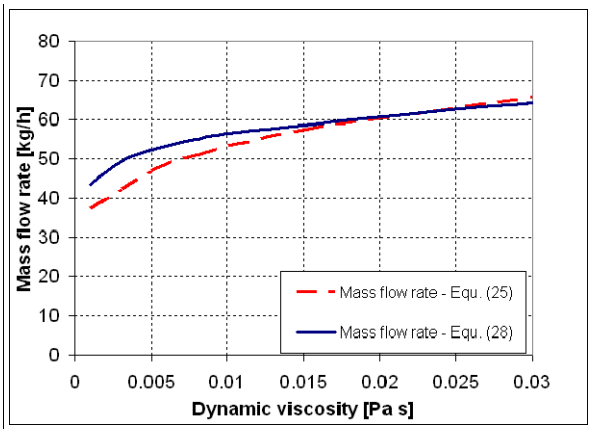

Figure 4. Discharge behaviour of the atomizer Delavan SB-30, at a pressure difference of 29 bar for different dynamic viscosities

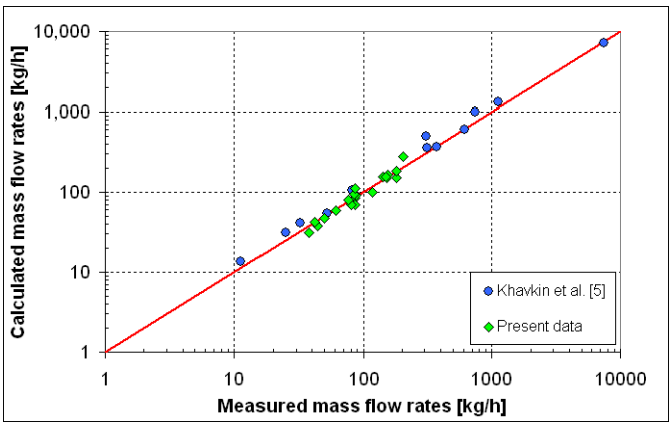

Figure 5. Comparison of the liquid mass flow rate calculated by eq. (25) with measured data for various liquids and atomizers (Tables 3 and 4)

In the present section we represent the measured liquid flow rates by our computational results. Additionally, we reproduce some measurement results from Khavkin et al. [6], which are listed in Table 4. The ranges of data covered in our experiments are listed in Table 3. Khavkin et al., who developed the theoretical description of the discharge behaviour of a pressure-swirl atomizer used in the present paper, show data on liquid throughput through an atomizer with flow rates varying by orders of magnitude. In all decades, the computations represent the data very well. The data in Fig. 5 show that this is the case for the atomizers of the present experiments as well. In particular the increase of the liquid flow rate through a given atomizer with the liquid dynamic viscosity for a constant driving pressure difference is represented correctly as a trend in the results.

As another important result of the above computations we obtain the radius of the air core around the symmetry axis of the swirl chamber as a function of the liquid throughput, the physical data of the liquid and the geometry of the atomizer. In Fig. 6 we show the evolution of the air core radius in the atomizer with the dynamic viscosity of the test liquid. It is seen that, with increasing liquid dynamic viscosity, the air core radius decreases. This indicates the increase of the cross section of the wall-bounded liquid film in the swirl chamber which puts the liquid flow through. This film thickness increase may be regarded as one important physical reason for the higher throughput.

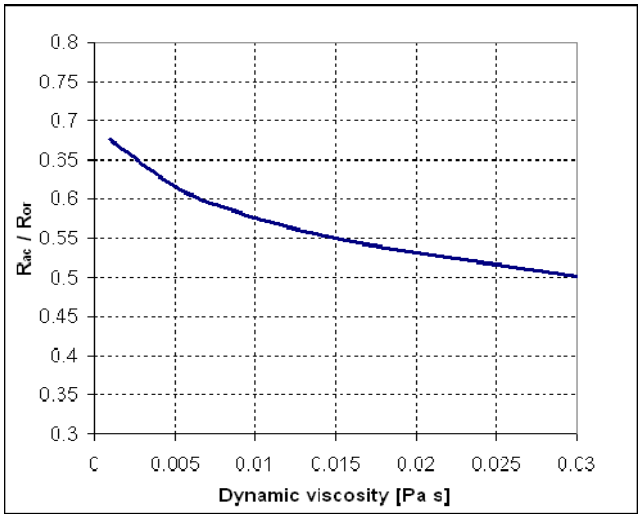

Figure 6. Calculated air core radius as a function of the dynamic viscosity of the test liquid for the atomizer Delavan SB-30, with a driving pressure difference of 29 bar

Table 3: Ranges of parameters in the experiments carried out on our test rig

Liquid density [kg/m³]	Liquid dynamic viscosity [Pa s]	Swirl chamber height L [mm]	Swirl chamber inlet area A_{in} [mm²]	R_{in} [mm]	Orifice radius R_{or} [mm]	Driving pressure difference [bar]	Measured liquid flow rate [kg/h]
1000 - 1039	0.001 - 0.030	1.88 - 8.1	1.98 - 25.1	3.4 - 5.6	0.381 - 1.143	2.2 - 57	38 - 204

Table 4: Experimental data and measurement results reproduced from Khavkin et al. [6]

Density [kg/m³]	Dynamic viscosity [Pa s]	Swirl chamber height L [mm]	Swirl chamber inlet area A_{in} [mm²]	R_{in} [mm]	Orifice radius R_{or} [mm]	Driving pressure difference [bar]	Measured liquid flow rate [kg/h]
1000	0.001	3	0.705	1.29	0.37	30	32.4
1000	0.001	3	0.705	1.29	0.3	30	25.2
1000	0.001	4	1.388	2.53	0.47	24.5	52.3
1000	0.001	3.5	0.192	2.33	0.25	20.1	11.4
1000	0.001	7.94	7.95	8.7	4.76	3	315
892	0.020	4	7.6	13.5	3.5	4	372.9
892	0.019	8	23.9	13.5	3.5	4	619.9
892	0.016	12	53.2	13.5	3.5	4	744.8
823	0.002	15.5	1.6	1.5	0.5	30	81.5
1000	0.001	6	7.08	4.75	1.5	35	307
892	0.015	24	54.2	8.5	3.5	4	1115
1000	0.001	1.5	102.1	21.2	8.4	20	7480

Summary and Conclusions

In the present contribution we compute the flow through the swirl chamber of a pressure-swirl atomizer with the aim to explain the experimental phenomenon that, at a given driving pressure difference, a liquid with a higher dynamic viscosity exhibits a higher throughput than a less viscous liquid, a fact that can safely be called counter-intuitive. The computations show that the radius of the air core is smaller for a liquid with higher viscosity, and that the flow rate through the wall-bounded liquid film is higher for the thicker film. The computational results are obtained with some coarse elements of modelling, which explain the slight scatter of the experimental data around the computed curve in Fig. 5. Despite this, the modelling, which followed the lines of Khavkin et al. [6] may be considered as satisfactory inasmuch as it describes correctly the phenomenon we focussed on. Further work in this direction will refine the modelling of the viscous losses in the contact zones of the liquid with the walls and may be complemented by numerical simulations of the flow field with the free surface at the air core. One further aim is to extend the modelling to viscosities above an optimal one where the flow rate tends to decrease with further increasing viscosity.

Acknowledgements

The authors acknowledge financial support of this work from BASF AG, GCP/TT, Ludwigshafen (Germany) and the excellent cooperation in the frame of the project.

References

[1] Taylor, G. I., *Quarterly Journal of Mechanics and Applied Mathematics* 3:129-139 (1950).
[2] Chinn, J. J., *Atomization and Sprays* 19: 263-282 (2009).
[3] Chinn, J. J., *Atomization and Sprays* 19: 283-308 (2009).
[4] Goldshtik, M. A., *Izvestija Akademija Nauk USSR, Series Mechanika i Mashinostroenie* 1: 132-137 (1963).
[5] Khavkin, Y., *Theory and Practice of Swirl Atomizers* Taylor & Francis (2004).
[6] Khavkin, Y., Strelkov, B. D., Nekhamkin, Y. E., *Teploenergetika* 10: 49-52 (1978).
[7] Novikov, B. W., *Teploenergetika* 5: 81-83 (1966).
[8] Khavkin, Y., *Mechanical Engineering*, (1976).
[9] Orzechowski, Z., *Liquid Atomization* WNT Warsaw (1976), as cited in [3].
[10] Tratnig, A., Brenn, G., *International Journal of Multiphase Flow* 36: 349-363 (2010).